Supplementary Information (SI) for ChemComm.


# High-area alumina supported Cu-Ce atomic species for water-gas shift reaction

Yiwei Yu,[a] Tie Wang,[b c] Ning Yan[b] and Jingyue Liu*[d]

[a] *School for Engineering of Matter, Transport and Energy, Arizona State University, Tempe, Arizona 85287, USA.*
[b] *Department of Chemical and Biomolecular Engineering, National University of Singapore, Singapore 117585, Singapore.*
[c] *Joint School of NUS and TJU, International Campus of Tianjin University, Fuzhou 350207, China*
[d] *Department of Physics, Arizona State University, Tempe, Arizona 85287, USA.*
*E-mail: Jingyue.liu@asu.edu

# 1 Experimental Section

## 1.1 Materials

Gamma alumina ($\gamma$-$Al_2O_3$) was purchased from US Research Nanomaterials. Disodium ethylenediaminetetraacetate dihydrate (EDTA-$Na_2$·$2H_2O$), cerium(III) nitrate hexahydrate ($Ce(NO_3)_3$·$6H_2O$), copper(II) nitrate trihydrate ($Cu(NO_3)_2$·$3H_2O$), ammonia solution ($NH_4OH$), and sodium hydroxide (NaOH) were purchased from Sigma-Aldrich. All reagents were used as received without further purification.

## 1.2 Synthesis of Cu-Ce/$\gamma$-$Al_2O_3$ and Cu/$\gamma$-$Al_2O_3$.

Prior to depositing the metal precursor species, the $\gamma$-$Al_2O_3$ powders were pretreated by immersion in a 0.1M ammonia solution to enhance the adsorption of atomically dispersed metal species.[1] A strong electrostatic adsorption (SEA) assisted deposition method was used for dispersing Ce and Cu precursor species onto high-area $\gamma$-$Al_2O_3$.[2,3] For deposition of Ce species, the precursor solution was prepared by dissolving 1.06 g of EDTA·$Na_2$ and 1.24 g $Ce(NO_3)_3$·$6H_2O$ in 150 mL of deionized water and tuning the solution pH to ~5 using 1M NaOH with stirring. In parallel, 1 g of pretreated $\gamma$-$Al_2O_3$ powders were dispersed into the 50 mL of deionized water via ultrasonication. The prepared salt precursor solution was then added, dropwise, to the $\gamma$-$Al_2O_3$ solution under vigorous stirring for an hour. The resulting solution mixture was subjected to centrifugation, with subsequent washing three times with deionized water. The resultant product was then dried overnight at 60 °C under vacuum and finally calcined at 300 °C in air for 3 hours, yielding Ce/$\gamma$-$Al_2O_3$.

The deposition of Cu species onto the above as-prepared Ce/$\gamma$-$Al_2O_3$ followed a similar procedure of preparing the Ce/$\gamma$-$Al_2O_3$: dissolving 0.29 g EDTA·$Na_2$ and 0.19 g $Cu(NO_3)_2$·$3H_2O$ in 150 mL of deionized water to prepare the precursor solution. Then, 1g of Ce/$\gamma$-$Al_2O_3$ powder was dispersed into 50 mL of deionized water via ultrasonication, followed by dropwise addition of the precursor for an hour under vigorous stirring. The resultant solution was filtered, washed, and calcined. The final product was denoted as Cu-Ce/$\gamma$-$Al_2O_3$. The deposition of Cu onto $\gamma$-$Al_2O_3$ followed the same procedure as that of preparing Cu onto Ce/$\gamma$-$Al_2O_3$. The final powder product was denoted as Cu/$\gamma$-$Al_2O_3$. A reference Cu-Ce/$\gamma$-$Al_2O_3$-ammonia sample was prepared using the same precursors and conditions as for Cu-Ce/$\gamma$-$Al_2O_3$ except replacing NaOH by ammonia solution.

A series of xCu-Ce/γ-$Al_2O_3$ (where x denotes the wt% Cu loading) with a fixed amount Ce loading were synthesized via the SEA method. Table S1 displays the synthesized catalysts and their corresponding nominal and actual (determined by ICP-MS) Cu loadings.

### 1.3 Catalyst Characterization

The loading amount of metal (Cu, Ce) in the Cu-Ce/γ-$Al_2O_3$ and Cu/γ-$Al_2O_3$ catalysts was determined by Thermo Scientific Quadrupole inductively coupled plasma mass spectrometry (ICP-MS). Powder X-ray diffraction (XRD) patterns were recorded on a Malvern PANalytical Aeris X-ray diffractometer using Cu Kα radiation (40 kV and 15 mA) with a step size of 0.01°. Backscattered electron (BSE) images were obtained on the JEOL JXA-8530F electron microprobe for examining the presence and distribution of large particles of heavy elements in the catalysts.[4] The samples were prepared via a multistep grind/polish method to acquire representative information.[5] Aberration-corrected scanning transmission electron microscopy (STEM) imaging was performed on a JEM-ARM200F to examine the configuration and spatial distribution of Ce and Cu species. X-ray photoelectron spectroscopy (XPS) data was collected on an Axis Supra+ (Kratos Analytical) analyzer, using a monochromated Al Kα X-ray source (=1486.6 eV). The binding energies (BEs) were calibrated using the C1s peak at 284.6 eV as a reference. Prior to collecting the XPS data, the catalyst powders were treated in 5% $H_2$/He with a flow rate of 10 ml/min at 300 °C for 1 hour and sealed in a reactor vessel to transfer to a nitrogen-filled glovebox for sample preparation. *In situ* diffuse reflectance infrared Fourier transform (DRIFT) spectra were recorded using an iS50 FT-IR spectrometer with a mercury-cadmium-telluride (MCT) detector and a Praying Mantis™ high-temperature reaction chamber with zinc selenide windows. For all spectra, 32 scans with a resolution of 4 $cm^{-1}$ were recorded at 25 °C. Before CO adsorption, each catalyst was reduced under 5% $H_2$ balanced with $N_2$ for 1 h at 300 °C and subsequently cooled down to 25 °C and pretreated with Ar for 20 min. The background was then recorded, followed by CO adsorption using 5% CO/Ar for 20 minutes until saturation. Subsequently, the sample was flushed with Ar to purge gas-phase CO from the environmental cell and the weakly adsorbed CO on the catalyst, the IR spectra were recorded continuously until the signal intensity was no longer decreased. All gases and gas mixtures were introduced at 10 mL/min at ambient pressure.

**1.4 Catalytic Performance Evaluation**

The WGSR was evaluated in a fixed-bed plug-flow reactor at atmospheric pressure. Typically, 50 mg of catalyst powders—packed between two quartz wool plugs inside a quartz tube (inner diameter of 4 mm)—were used for WGSR. Prior to each test, the catalyst powders were treated in 5% $H_2$/He with a flow rate of 10 ml/min at 300 °C for 1 hour. The WGSR feed gas contains 1% CO, 10% $H_2O$ and He balance; the flow rate of the gas mixture was controlled to be 62 ml·min$^{-1}$, yielding a space velocity (SV) of 74,400 ml·g$^{-1}$·h$^{-1}$. The temperature of the catalyst bed was then raised to the desired reaction temperature with a ramping rate of 2 °C·min$^{-1}$. The concentrations of CO in the outlet stream were measured by an online gas chromatograph (Agilent 7890A) equipped with a thermal conductivity detector. The CO conversion ($X_{CO}$) and specific activity (r) is calculated by:

$$X_{CO}\ (\%) = \frac{[CO]_{in} - [CO]_{out}}{[CO]_{in}} \times 100$$

$$r = X_{CO} \times [CO]_{in} \times SV$$

where the subscript "in" and "out" indicate the concentration of the inlet and outlet CO gaseous stream. The unit for *r* is in [μmol $g_{cat}^{-1}$ $s^{-1}$]. CO conversion datapoints recorded at the conversion less than 20% will be used to calculate the activation energy. The temperature dependent reaction rate constant of chemical reactions can be interpreted corresponding to Arrhenius equation:

$$k\ =\ Ae^{-E_a/RT}$$

Where *k* is the rate constant, *A* is the pre-exponential factor (constant for each chemical reaction), $E_a$ is the activation energy, *R* is the gas constant, and *T* is the absolute temperature. For a reaction between X and Y (mX+ nY → products) in a small temperature range, the reaction rate can be expressed as:

$$r\ =\ k\,[X]^m[Y]^n\ =\ A\,[X]^m[Y]^n\,e^{-E_a/RT}$$

Then,

$$\ln(r) = -\frac{E_a}{RT} + m\ln[x] + n\,ln[Y] + lnA = -\frac{E_a}{RT} + C$$

Where *C* is a constant.

By plotting $\ln(r)$ vs 1000/T ($K^{-1}$), the value of $E_a$ can be obtained as -slope×8.314 (kJ $mol^{-1}$).

## 2. Supplementary Figures

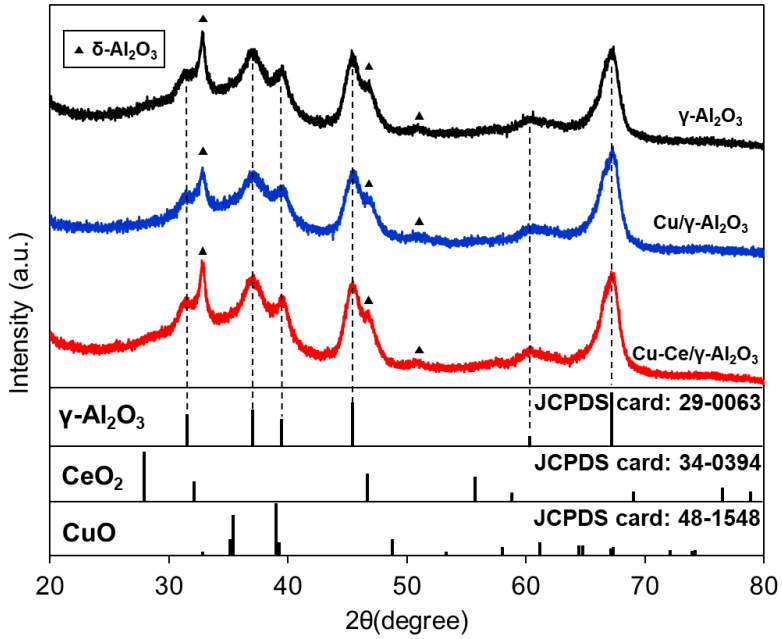


**Figure S1.** XRD patterns of the γ-$Al_2O_3$ support, as-prepared Cu/γ-$Al_2O_3$ and Cu-Ce/γ-$Al_2O_3$ samples. The XRD patterns of Cu/γ-$Al_2O_3$ and Cu-Ce/γ-$Al_2O_3$ exhibit almost the same peaks corresponding to γ-$Al_2O_3$ and δ-$Al_2O_3$.[6] The absence of recognizable characteristic peaks characterizing Cu- and Ce-related phases suggests lack of crystalline particles, except the γ-$Al_2O_3$, in the Cu/γ-$Al_2O_3$ and Cu-Ce/γ-$Al_2O_3$ catalysts. Electron microscopy results corroborate this conclusion.

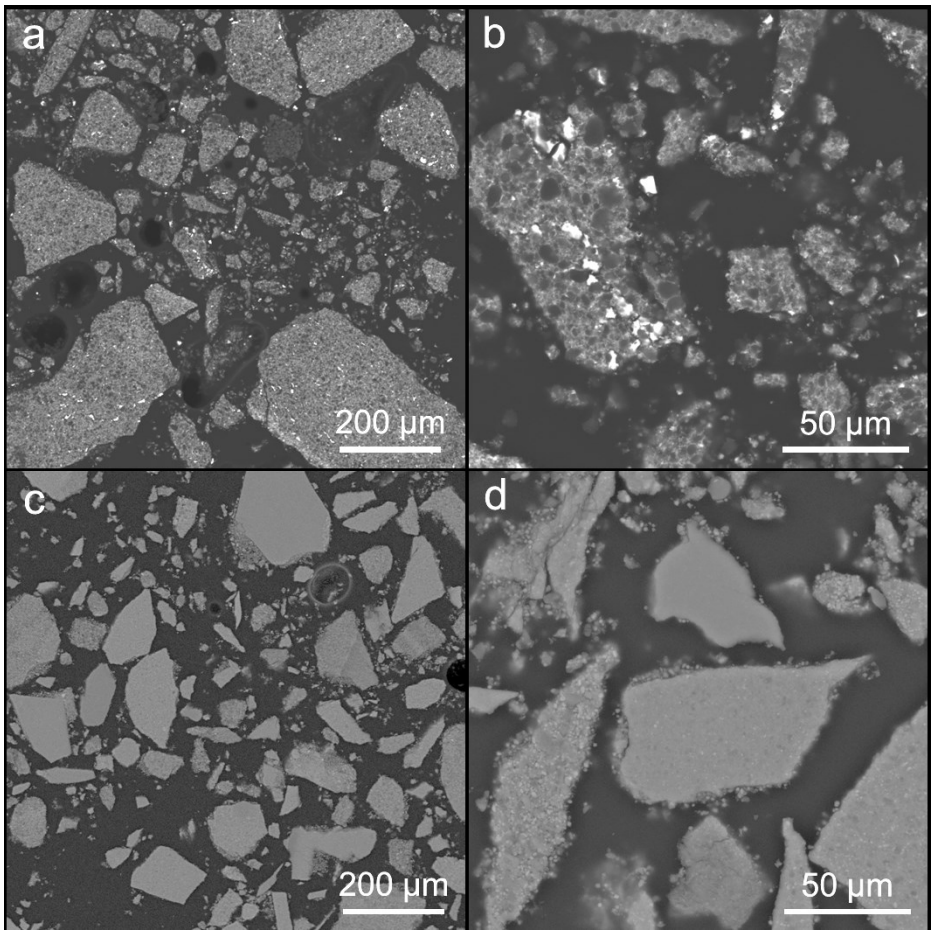


**Figure S2.** (a) (b) BSE images of a γ-$Al_2O_3$ supported ceria sample prepared via a precipitation method reveal various sizes of large ceria particles/agglomerates. (c) (d) BSE images of the as-prepared Cu-Ce/γ-$Al_2O_3$ sample shows absence of Cu- or Ce-related particles/agglomerates.

Large ceria or copper oxide particles/agglomerates should be easily revealed with bright contrast in BSE images (Fig. S2 (a, b)).[4]

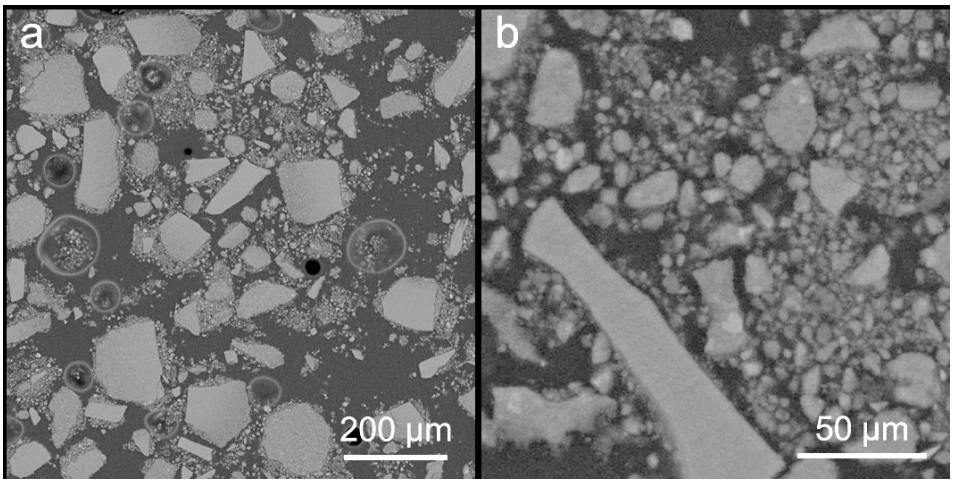


**Figure S3.** (a, b) BSE images of Cu/γ-$Al_2O_3$ show absence of large Cu-related particles.

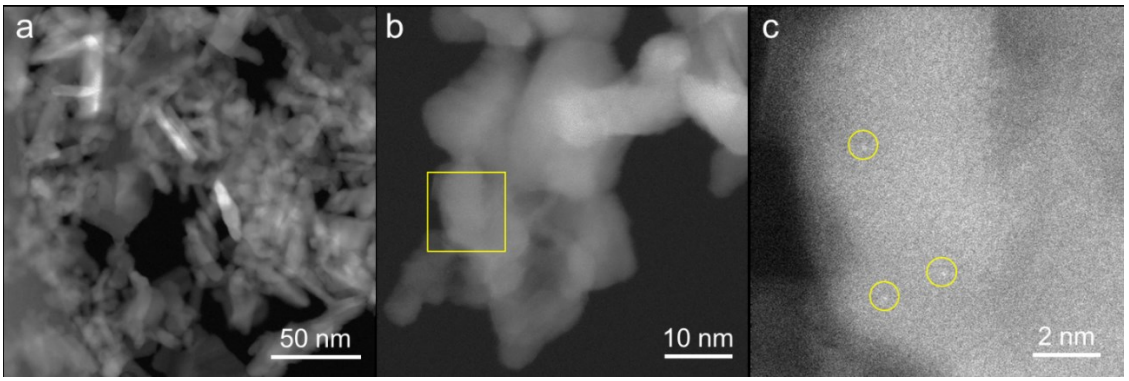


**Figure S4.** Low magnification HAADF-STEM images (a, b) of the Cu/γ-$Al_2O_3$ sample show absence of particles/clusters of Cu phases. (c) Atomic resolution HAADF-STEM image of the selected area marked by the yellow box in (b) shows isolated Cu atoms.

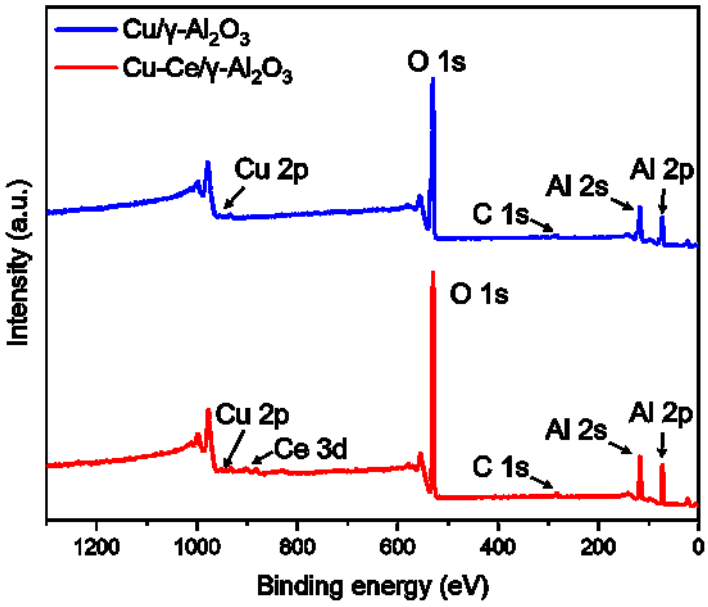


**Figure S5.** XPS wide-scan spectra over the Cu/γ-$Al_2O_3$ and Cu-Ce/γ-$Al_2O_3$ catalyst powders. The spectra indicate the presence of Cu, O, C and Al in both Cu/γ-$Al_2O_3$ and Cu-Ce/γ-$Al_2O_3$ samples and Ce in the Cu-Ce/γ-$Al_2O_3$ sample.

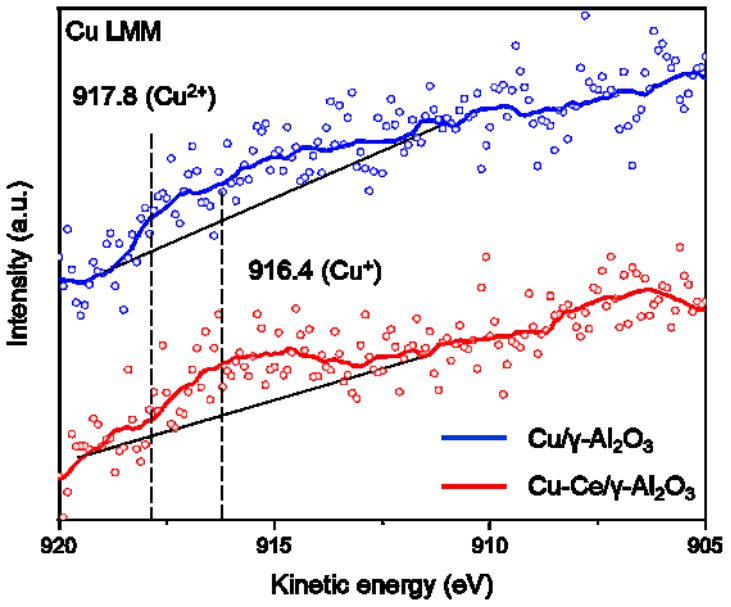


**Figure S6.** XPS Cu LMM Auger spectra characterizing Cu/γ-$Al_2O_3$ and Cu-Ce/γ-$Al_2O_3$ samples show the presence of $Cu^+$ and $Cu^{2+}$ in both samples. No characteristic peak (~918.8 eV) of the $Cu^0$ species was observed in both samples.[7]

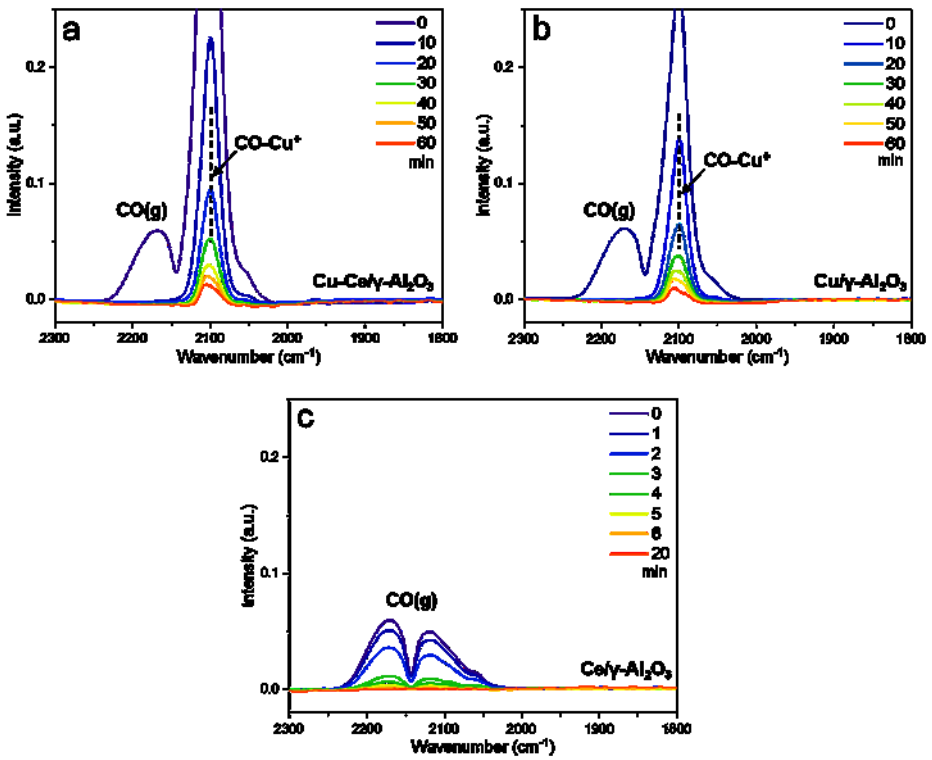


**Figure S7.** *In-situ* DRIFT spectra over (a) Cu-Ce/γ-$Al_2O_3$, (b) Cu/γ-$Al_2O_3$ and (c) Ce/γ-$Al_2O_3$. The catalysts were first reduced by 5% $H_2$ at 300°C for 1h prior to CO adsorption, and then purged with Ar and simultaneously the DRIFT signals were recorded at 25 °C. Only gas-phase CO bands are present over the Ce/γ-$Al_2O_3$ control catalyst, reflecting poor CO adsorption on atomically dispersed Ce species. The predominant bands at 2090–2110 $cm^{-1}$ in the spectra over the Cu/γ-$Al_2O_3$ and Cu-Ce/γ-$Al_2O_3$ catalysts can be assigned to the C-O stretching vibration peaks of $Cu^+$-CO.[8] After 60 min of argon purging, the absorption bands over the Cu-Ce/γ-$Al_2O_3$ showed higher intensity than those over the Cu/γ-$Al_2O_3$, suggesting higher amount of adsorbed CO on the Cu-Ce/γ-$Al_2O_3$ than that on the Cu/γ-$Al_2O_3$ catalyst. The presence of the small shoulder peak at the lower frequency (~2095 $cm^{-1}$) might be ascribed to CO adsorbed on $Cu^+$ sites with a less oxidized environment.[9]

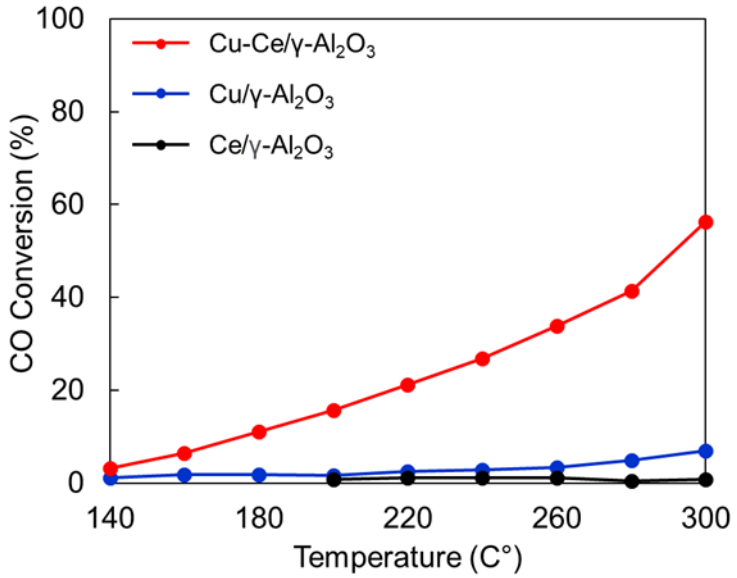


**Figure S8.** CO conversion rate as a function of WGSR temperature. Reaction condition: 1% CO + 10% $H_2O$ and He balance, SV=74,400 ml $g^{-1}$ $h^{-1}$.

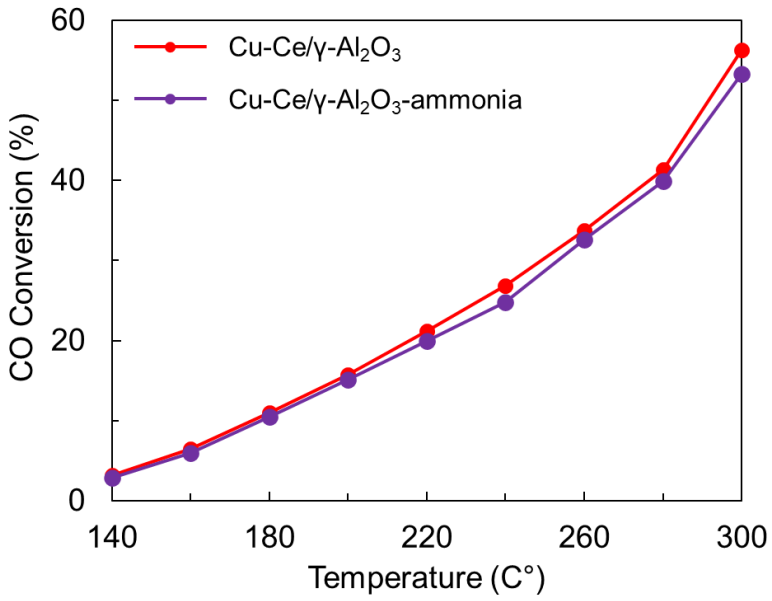


**Figure S9.** Plots of CO conversion rate vs. temperature for WGSR over the Cu-Ce/γ-$Al_2O_3$ (synthesized by use of NaOH and DI water wash) and the Cu-Ce/γ-$Al_2O_3$-ammonia (synthesized by use of ammonia) catalysts. The potential impact of Na ion residue in the Cu-Ce/γ-$Al_2O_3$ catalyst on the WGSR activity can be considered insignificant. Reaction condition: 1% CO +10% $H_2O$+He balance, SV=74,400 ml $g^{-1}$ $h^{-1}$.

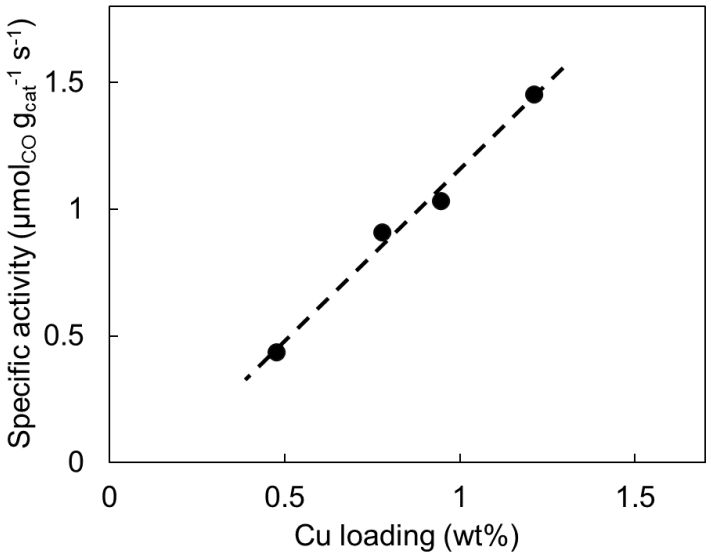


**Figure S10.** WGSR reaction rate at 200 °C as a function of Cu loading level for xCu-Ce/γ-$Al_2O_3$ catalysts. Since the atomically dispersed Ce species do not provide appreciable activity, for low Cu loading levels the experimentally obtained WGSR activity should be directly proportional to the total amount of Cu loading.[10] The nearly linear increases in the specific activity of the WGSR with the total number of Cu atoms in the Cu-Ce/γ-$Al_2O_3$ catalyst suggests that the Cu species were most likely atomically dispersed or isolated from each other.

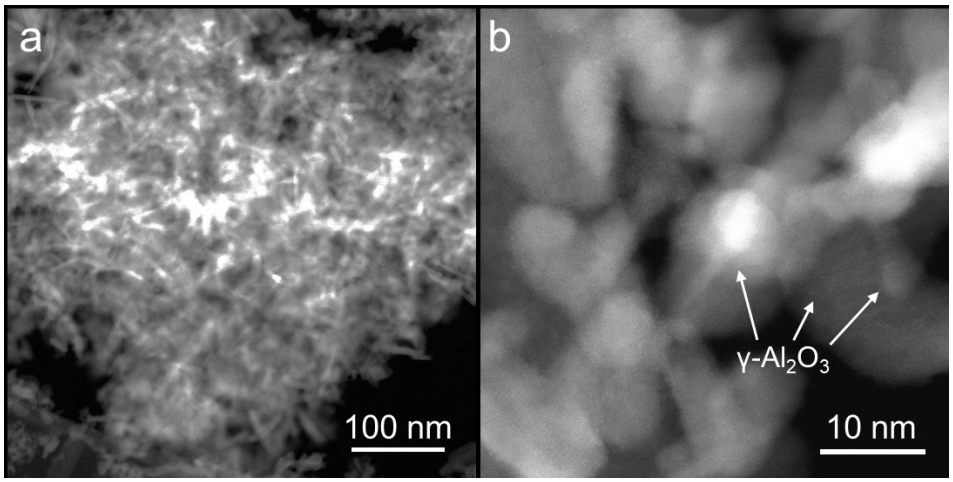


**Figure S11.** HAADF-STEM images of the Cu/γ-$Al_2O_3$ catalyst, after the WGSR stability test, confirm absence of Cu clusters/particles.

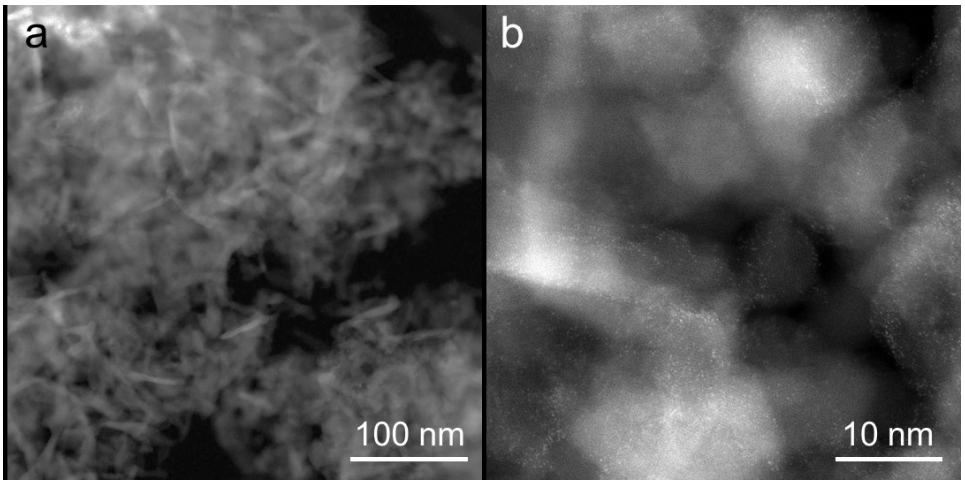


**Figure S12.** HAADF-STEM images of Cu-Ce/γ-$Al_2O_3$ samples after WGS stability test show absence of metal clusters/particles and the presence of atomically dispersed Ce and Cu species.

## 3. Supplementary Tables

Table S1. Catalyst name, nominal loading, and actual loading (determined by ICP-MS) for catalysts prepared with different amount of Cu precursor on a 2.6 wt% Ce/γ-$Al_2O_3$ support.

| Catalyst name | Nominal loading (wt%) | Actual loading (wt%) |
|---|---|---|
| 1.2Cu-Ce/γ-$Al_2O_3$ | 5.0 | 1.2 |
| 0.94Cu-Ce/γ-$Al_2O_3$ | 1.3 | 0.94 |
| 0.78Cu-Ce/γ-$Al_2O_3$ | 0.8 | 0.78 |
| 0.48Cu-Ce/γ-$Al_2O_3$ | 0.5 | 0.48 |

Table S2. WGSR activity over our Cu-Ce/γ-$Al_2O_3$ and Cu/γ-$Al_2O_3$ catalysts in comparison to those copper-ceria catalysts reported in literature.

| Sample name | Cu wt% | Specific activity* (μmol $g_{cat}^{-1}$ $s^{-1}$) | Reference |
|---|---|---|---|
| Cu-Ce/γ-$Al_2O_3$ | 1.2 | 1.4 | This work |
| Cu/γ-$Al_2O_3$ | 1.4 | 0.16 | This work |
| 1.5CuCe-CP-L | 1.5 | 0.37 | [11] |
| 8.2CuCe-CP | 8.2 | 3.0 | [11] |
| 8 wt.% Cu–$CeO_2$ | 8.0 | 0.11 | [12] |
| $Cu_{0.15}Ce_{0.85}O_x$ | 15 | 12 | [13] |
| $CeO_2$/Cu | 83 | 10 | [14]** |
| Cu-473 | 3.4 | 5.0 | [15] |
| Cu-P | 1.6 | 2.2 | [16]*** |
| Cu-C | 1.5 | 1.2 | [16] |
| Cu-R | 1.6 | 0.8 | [16] |

* Measured at 200 °C.
** Highest WGSR activity (if measured at 300 °C) among all Cu-based catalysts.
*** Atomically dispersed Cu on $CeO_2$ particles

## 4. References


1 J. Zhang, J. Chen, J. Ren and Y. Sun, *Appl. Catal., A*, 2003, **243**, 121–133.

2 X. Li, X. I. Pereira-Hernández, Y. Chen, J. Xu, J. Zhao, C.-W. Pao, C.-Y. Fang, J. Zeng, Y. Wang, B. C. Gates and J. Liu, *Nature*, 2022, **611**, 284–288.

3 A. Wong, Q. Liu, S. Griffin, A. Nicholls and J. R. Regalbuto, *Science*, 2017, **358**, 1427–1430.

4 J. Liu, *Microsc. Microanal.*, 2000, **6**, 388–399.

5 Y. Yu, C. Zhu, B. Zhao, P.-X. Gao and J. Liu, *Microsc. Microanal.*, 2023, **29**, 124–125.

6 A. A. Vedyagin, R. M. Kenzhin, M. Yu. Tashlanov, E. A. Alikin, V. O. Stoyanovskii, P. E. Plyusnin, Y. V. Shubin, I. V. Mishakov, M. Yu. Smirnov, A. V. Kalinkin and V. I. Bukhtiyarov, *Top Catal.*, 2020, **63**, 152–165.

7 S. Poulston, P. M. Parlett, P. Stone and M. Bowker, *Surf. Interface Anal.*, 1996, **24**, 811–820.

8 H. Wan, Z. Wang, J. Zhu, X. Li, B. Liu, F. Gao, L. Dong and Y. Chen, *Applied Catalysis B: Environmental*, 2008, **79**, 254–261. A. Martínez-Arias, R. Cataluña, J. C. Conesa and J. Soria, *J. Phys. Chem. B*, 1998, **102**, 809–817.

9 A. Martínez-Arias, R. Cataluña, J. C. Conesa and J. Soria, *J. Phys. Chem. B*, 1998, **102**, 809–817.

10 X.-F. Yang, A. Wang, B. Qiao, J. Li, J. Liu and T. Zhang, *Acc. Chem. Res.*, 2013, **46**, 1740–1748.

11 R. Si, J. Raitano, N. Yi, L. Zhang, S.-W. Chan and M. Flytzani-Stephanopoulos, *Catal. Today*, 2012, **180**, 68–80.

12 N. A. Koryabkina, A. A. Phatak, W. F. Ruettinger, R. J. Farrauto and F. H. Ribeiro, *J. Catal.* 2003, **217**, 233–239.

13 A. Pintar, J. Batista and S. Hočevar, *J. Colloid Interface Sci.*, 2007, **307**, 145–157.

14 H. Yan, C. Yang, W.-P. Shao, L.-H. Cai, W.-W. Wang, Z. Jin and C.-J. Jia, *Nat. Commun.*, 2019, **10**, 3470.

15 A. Chen, X. Yu, Y. Zhou, S. Miao, Y. Li, S. Kuld, J. Sehested, J. Liu, T. Aoki, S. Hong, M. F. Camellone, S. Fabris, J. Ning, C. Jin, C. Yang, A. Nefedov, C. Wöll, Y. Wang and W. Shen, *Nat. Catal.*, 2019, **2**, 334–341.

16 J. Ning, Y. Zhou and W. Shen, *Sci. China Chem.*, 2021, **64***,* 1103–1110.